Volume 4

Chapter 17

https://doi.org/10.32685/pub.esp.38.2019.17
Published online 26 June 2020

Integrated Perspective of the Present–Day Stress and Strain Regime in Colombia from Analysis of Earthquake Focal Mechanisms and Geodetic Data

Mónica ARCILA[1]* and Alfonso MUÑOZ–MARTÍN[2]

1 marcila@sgc.gov.co
mmarcila@ucm.es
Servicio Geológico Colombiano
Dirección de Geoamenazas
Diagonal 53 n.° 34–53
Bogotá, Colombia
Universidad Complutense de Madrid
Avenida José Antonio Novais, 12
Madrid, España

2 amunoz@ucm.es
Universidad Complutense de Madrid
Avenida José Antonio Novais, 12
Madrid, España

* Corresponding author

Supplementary Information:
S: https://www2.sgc.gov.co/LibroGeologiaColombia/tgc/sgcpubesp38201917s.pdf

Abstract Focal mechanism analysis is a powerful tool for analyzing the geodynamic context of broad and complex regions, such as northwestern South America. In this zone, a complex tectonic convergence occurs among the Caribbean, Nazca, and South American Plates. The orientations of the maximum horizontal shortening and the values of the brittle strain/stress regime (k' ratio) are obtained based on the analysis of 617 centroid–moment tensors reported from 1976 to 2017 in the Global Centroid–Moment–Tensor Project. These results are complemented with an analysis of GPS velocities, which can be used to determine the surficial deformation and to compare it with the crustal deformation to define the stress field in Colombia, and to formulate a seismotectonic model. This model is characterized by the slow southeastwards displacement of the Caribbean Plate, the convergence of the Andean, Coiba, and Panamá Blocks in northwestern Colombia, and the westwards convergence of the Nazca Plate below the South American overriding Plate. The strain/stress regime maps also show different tectonic environments and large–scale geological heterogeneities.

Keywords: *Andean, active stress, strain, focal mechanism, GPS velocities.*

Resumen El análisis de mecanismos focales es una herramienta poderosa para analizar el contexto geodinámico de regiones extensas y complejas, como la esquina noroccidental de Suramérica. En esta zona se produce una compleja convergencia tectónica entre las placas del Caribe, de Nazca y de Suramérica. Los valores para la dirección de máximo acortamiento horizontal y el régimen frágil de esfuerzo/deformación (k') son obtenidos para el análisis de 617 tensores de momento sísmico reportados desde 1976 hasta 2017 en el Global Centroid–Moment–Tensor Project. Estos resultados se complementan con un análisis de las velocidades GPS, que permite analizar la deformación superficial, y compararla con la deformación de la corteza, para definir el campo de esfuerzos en Colombia y formular un modelo sismotectónico. Este modelo está caracterizado por un lento desplazamiento hacia el sureste de la Placa del Caribe, la convergencia de los bloques Andino, Coiba y Panamá en el noroeste de Colombia y la convergencia hacia el oeste de la Placa de Nazca por debajo de la Placa de Suramé-

Citation: Arcila, M. & Muñoz–Martín, A. 2020. Integrated perspective of the present–day stress and strain regime in Colombia from analysis of earthquake focal mechanisms and geodetic data. In: Gómez, J. & Pinilla–Pachon, A.O. (editors), The Geology of Colombia, Volume 4 Quaternary. Servicio Geológico Colombiano, Publicaciones Geológicas Especiales 38, p. 549–569. Bogotá. https://doi.org/10.32685/pub.esp.38.2019.17

rica cabalgante. Los mapas de régimen de esfuerzo/deformación también muestran diferentes ambientes tectónicos y heterogeneidades geológicas de gran escala.
Palabras clave: *andino, esfuerzo activo, deformación, mecanismo focal, velocidades GPS.*

1. Introduction and Objectives

Understanding the current stress and strain states at regional and local scales has fundamental value in seismic hazard assessments and practical applications such as the opening and operation of tunnels and the drilling and exploration of wells for oil and water. This chapter offers a regional view of the Colombian tectonic context from comparative analyses of the active crustal stresses deduced from earthquake focal mechanisms and the strain rates determined by spatial geodetic techniques (e.g., the Global Positioning System, GPS).

On a global scale, stress patterns are related to the tectonic processes and kinematics of lithospheric plates, and they are often consistent across large areas. The general features of the Colombian tectonic context, which are marked by the convergence of the Caribbean, Nazca, and South American Plates in northwestern South America, can be seen in the distribution of seismicity (Figure 1) (Engdahl et al., 1998; International Seismological Centre, 2019; Weston et al., 2018). This seismicity generally indicates the plate boundaries, the process of subduction in the Pacific, and regions of shallow seismicity within Colombia.

Initiatives such as the World Stress Map project, which consists of a global compilation of information about the current crustal stress field (Heidbach et al., 2016; Zoback, 1992; Zoback et al., 1989), have developed fairly generalized maps of the global pattern. Regional analyses of the trajectories of the maximum horizontal stress for northwestern South America can be found in the geodynamic studies conducted by Stephan (1982) and Stephan et al. (1986) and resumed by Audemard & Audemard (2002).

Research has also focused on the stress and strain states in certain regions of Colombia, including the work carried out by Rivera (1989) and Salcedo–Hurtado (1995), who studied the intermediate–depth "seismic nest" of Bucaramanga (Santander Department); Cardona et al. (2005) and Salcedo–Hurtado (1995) and who investigated the northwestern zone of Colombia based on focal mechanisms and GPS data; Dimaté et al. (2003), who studied the Tauramena earthquake (Casanare Department, 19 January 1995) based on an analysis of earthquake focal mechanisms; and Egbue et al. (2014), who analyzed the evolution of the stress and strain fields in the Eastern Cordillera considering paleostresses and integrating orientations of the present–day field determined via GPS, earthquake focal mechanisms, and borehole breakouts.

Arcila et al. (2000a, 2000b, 2002) integrated the results of current tectonic stresses obtained from the analysis of earthquake focal mechanism populations combined with lithospheric plate displacement data obtained via GPS. The results obtained by these authors reflect the stress fields in the Colombian territory and can be used by researchers to formulate a seismotectonic scheme for the convergence of lithospheric plates at the northwestern corner of South America. Vargas et al. (2002) analyzed the stress state in Colombia from satellite geodesy results and earthquake focal mechanisms from the Harvard catalog, now the Global Centroid–Moment–Tensor (CMT) Project (Dziewonski et al., 1981; Ekström et al., 2012), and obtained conclusions for the Chocó Block slightly different from those proposed by some authors. Colmenares & Zoback (2003) integrated in situ stress data with neotectonic and GPS data to examine the different seismotectonic models proposed for northern South America. Corredor (2003) estimated the seismic strain rates in five subregions of Colombia from the components of the seismic moment tensor of the earthquakes recorded in the Harvard catalog database (now the global CMT), finding matches with previous tectonic models and with models of relative plate motions.

The results of in situ stress measurements in wells and engineering works are scarce and not very accessible to the scientific community. However, certain results have been presented by Castillo & Mojica (1990) for the Eastern Cordillera in Colombia.

Using another approach, some researchers (e.g., Kreemer et al., 2014) have also analyzed surface strain from a global perspective from GPS data, which can yield rates and patterns of crustal deformation. At the regional level, workers have used the SIRGAS network (Sistema de Referencia Geocéntrico para las Américas) to periodically generate displacement velocity models based on the multiyear solutions from Global Navigation Satellite System (GNSS) stations. The most recent work is the solution SIR15P01, which was used to derive the velocity model VEMOS2015 (Sánchez & Drewes, 2016a).

For northwestern South America, several studies have been published that incorporate measurements of the displacement vectors of lithospheric plates based on both paleomagnetic information (e.g., DeMets et al., 2010) and GPS stations (e.g.,

→

Figure 1. Regional tectonic elements. The limits of plates and faults are modified from Veloza et al. (2012), seismicity from Weston et al. (2018) following the methodology and recommendations of Engdahl et al. (1998) and the locations of volcanoes from the Global Volcanism Program (2013). The inset marks the study area.

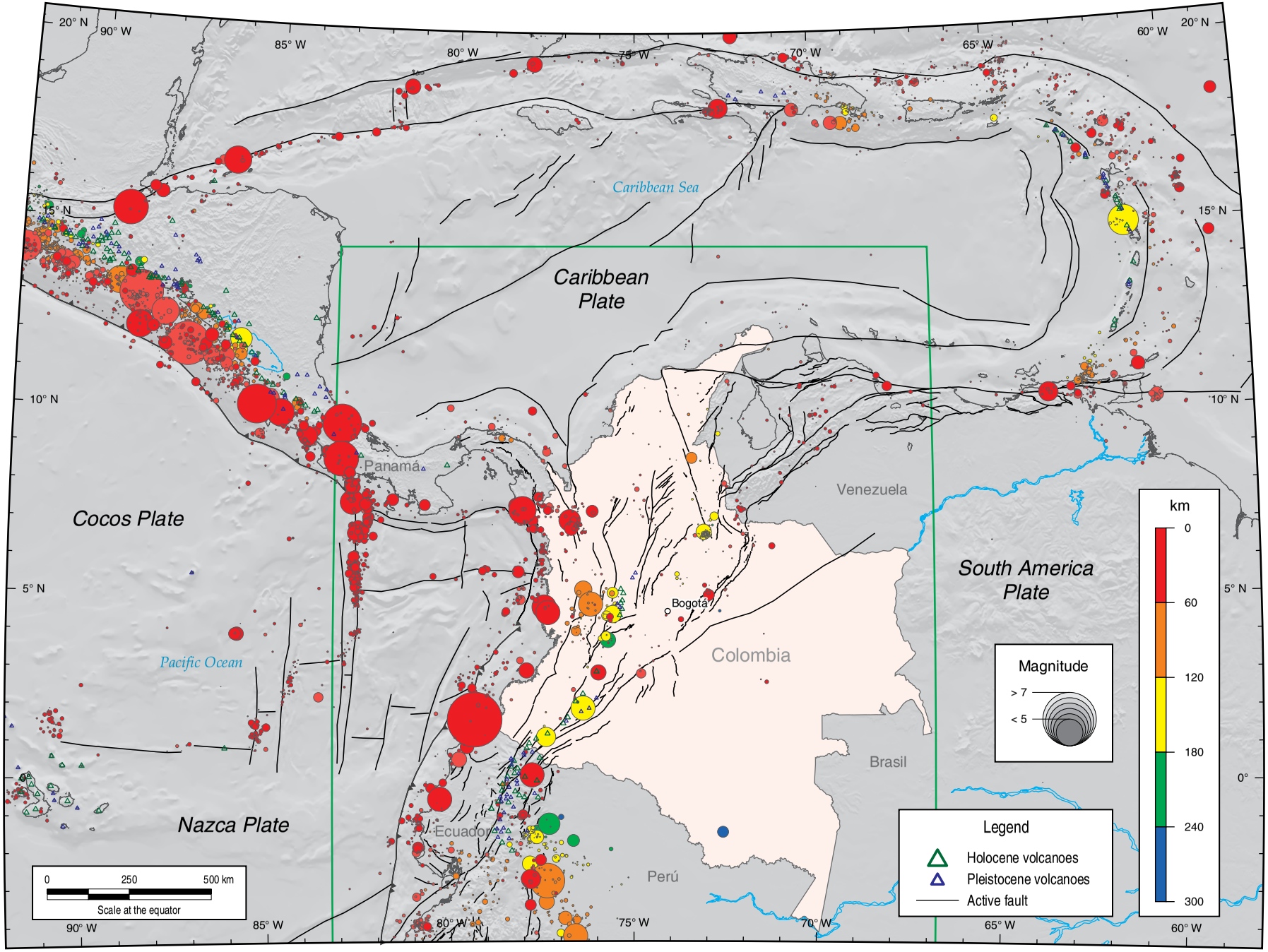
Caribbean Sea
Caribbean Plate
Cocos Plate
Nazca Plate
South America Plate
Pacific Ocean
Panamá
Venezuela
Colombia
Ecuador
Perú
Brasil
Bogotá
20° N
15° N
10° N
5° N
0°
90° W
85° W
80° W
75° W
70° W
65° W
60° W
km
0
60
120
180
240
300
Magnitude
> 7
< 5
Legend
Holocene volcanoes
Pleistocene volcanoes
Active fault
0
250
500 km
Scale at the equator

Freymueller et al., 1993; Kellogg & Vega, 1995) and that incorporate infrastructure information from Servicio Geológico Colombiano stations (Trenkamp et al., 2002).

In summary, researchers have most frequently used data consisting of earthquake focal mechanisms, the global CMT catalog, and displacements measured with geodetic techniques (especially GPS).

To determine the orientation of the stress and strain fields in Colombian territory, this work also resorts to these sources of information but differs in its methodologies. The advantage of using earthquake focal mechanisms is that they are the only available source of information on the active deformation process that provides data at a crustal scale and presents sufficient spatial distribution throughout the study area; however, the application of this technique is limited in areas of low seismicity. In addition, GPS data allow the quantification of the strain rates at the Earth's surface and have sufficient spatial distribution; however, these data are limited to the near–surface strain.

2. Methodology

This research presents two approaches to study the orientation of the current stress and deformation fields in northwestern South America, with an emphasis on the territory of Colombia. Traditionally, crustal deformation on a regional or global scale is studied using different approaches, many of which apply discrete data to generate continuous models of the deformation field. In this study, the first approach uses the orientation of the maximum horizontal compression and the shape of deformation of the focal mechanisms recorded in the global CMT catalog (Dziewonski et al., 1981; Ekström et al., 2012). The second approach utilizes the strain derived from the field of horizontal velocities obtained from GNSS (including GPS) data.

2.1. Stress States from Earthquake Focal Mechanisms

Traditionally, researchers have used focal mechanisms to establish related stress fields by defining the P (compression) and T (tension) axes. The main problem is that the P and T axes are not necessarily parallel to the principal axes of tectonic stress since the P and T axes represent only the orientations in which the earthquake radiates more energy (McKenzie, 1969). In fact, the P axis can be arranged in any position within the dilatational quadrant depending on the rheological conditions and the shape factor (regime) of the stress ellipsoid (Angelier, 1994).

Numerous works have demonstrated that nodal plane solutions for focal mechanisms are useful for defining the orientation of the stress field and provide information on the states of the stress and strain regimes. These states are usually defined by an ellipsoid shape factor.

Anderson (1951) proposed a classification of tectonic stress regimes in normal, compressive, and shear regimes, and he assumed that since there is no shear stress on the surface of the Earth (shear stress cannot occur in fluids), one of the principal stresses must be vertical, which implies that the other two are horizontal. The type of active regime is defined according to the vertical axis.

The methodology proposed by Capote et al. (1991) based on the slip model (De Vicente, 1988; Reches, 1978, 1983) was applied to calculate the orientation and shape factor of the deformation ellipsoid. This method, based on the Navier–Coulomb fracture criterion, assumes that the brittle strain and stress axes are parallel and that one of the axes is close to vertical. According to the slip model, under the triaxial strain conditions of brittle strain, fractures are arranged in orthorhombic symmetry with respect to the fundamental axes of the strain ellipsoid.

The slip model assumes that in the most general case (triaxial strain), the faults are arranged in four families, with two opposite directions and dips because these geometries are the best at dissipating energy during brittle strain. For slippage to occur, the cohesive and frictional resistance must be overcome. Although the slip model was developed from triaxial experiments via the generation of new fractures, numerous works have shown that the results obtained via analyses of populations of reactivated faults provide solutions similar to those of inversion methods that follow the Bott (1959) equation (e.g., Muñoz–Martín et al., 1998).

The model mathematically relates the shape of the strain ellipsoid (k') and the internal friction angle (ϕ) with the direction cosines of the slip striae and of the slip normal to the fault plane. The shape of the strain ellipsoid is given by the parameter k':

$$k' = \frac{e_y}{e_z}$$

where e_z is the axis of vertical strain and e_y is the axis of maximum horizontal shortening.

Two sequences of strain are established as functions of k', from reverse to normal sequences through strike–slip (Figure 2).

In this way, the orientation of maximum horizontal shortening (De_y), the internal friction angle during the slip (ϕ), and the shape factor of the ellipsoid e_y/e_z (k') are directly obtained for each event. The thirteen ellipsoid types as a function of the parameter k' are defined in Table 1.

In the case of earthquake focal mechanisms, if the two planes have different geometries (the relationship between the dip and pitch of the plane), then one plane exhibits motion with a normal component, and the other exhibits motion with a reverse component. The nodal plane, whose motion coincides with the character of the mechanism (normal or reverse), is the one that best dissipates frictional energy. This method allows the selection of the nodal plane of the focal mechanism for

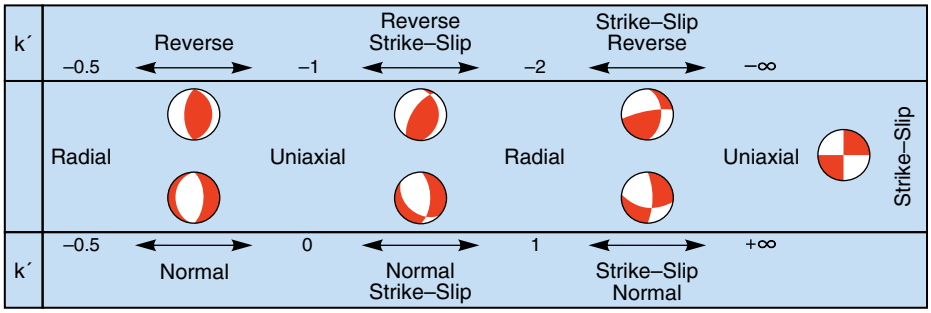

Figure 2. Diagram of stress regimes defined from the ellipsoid shape factor (k').

Table 1. Stress regimes defined by the shape factor of the strain ellipsoid (k').

	Shape factor (k')	Strain ellipsoid	Axis values	Fault type
	$k' = +\infty$	Planar deformation	$(e_z = 0; -e_x = e_y)$	Pure shear (R = 0)
	$+\infty > k' > 1$	Shear strain with extensional component	$(-e_x > e_y > e_z)$	Normal shear
	$k' = 1$		$(-e_x > e_y = e_z)$	
Normal sequence	$1 > k' > 0$	Extensional deformation with shear component	$(-e_x > e_z > e_y)$	Oblique normal ($R \neq 0, \neq 90$)
	$k' = 0$	(planar deformation)	$(-e_x = e_z; e_y = 0)$	
	$0 > k' > -0.5$	Extensional radial deformation	$(-e_z > -e_x > -e_y)$	Pure normal (R = 90)
	$k' = -0.5$	True extensional radial deformation	$(e_z > -e_x = -e_y)$ $(-e_Z > e_x = e_y)$	
	$-1 > k' > -0.5$	Compressional radial deformation	$(-e_z > e_y > e_x)$	Pure reverse (R = 90)
	$k' = -1$	(planar deformation)	$(-e_z = e_y; e_x = 0)$	
Reverse sequence	$-2 < k' < -1$	Compressional deformation with shear component	$(e_y > -e_z > -e_x)$	Oblique reverse ($R \neq 0, \neq 90$)
	$k' = -2$		$(e_y > -e_x = -e_z)$	
	$-\infty < k' < -2$	Shear stress with compressional component	$(e_y > -e_x > -e_z)$	Reverse shear
	$k' = -\infty$	Planar deformation	$(e_y = -e_x; e_z = 0)$	Pure shear (R = 0)

slippage on a fault by considering mechanical criteria. In this work, we have selected the plane that mechanically best suits each earthquake, and the results allow the establishment of the stress tensor characteristics.

Compared with the population analysis based on the Bott equation (Angelier, 1994; Delvaux & Sperner, 2003; Reches et al., 1992), the main advantage of the slip model considered in this focal mechanism analysis is that by identifying a solution for each earthquake (e.g., the directions of the horizontal stress axes and the shape factor k'), a better analysis of the available data can be performed due to a greater number of data and a more complete spatial distribution. This methodology has been shown to be very useful at different scales, ranging from the Iberian Peninsula (De Vicente et al., 2008) to all of Europe (Olaiz et al., 2009).

Data on focal mechanisms (from 1976) include only moderate to large events (in general Mw ≥ 5.0), and although the distribution and coverage for the territory may be limited, a rigorous analysis of the data can produce a picture of the present–day stress field. This information is fundamental to understanding the tectonic processes and stress states that currently prevail in the enormously complex zone associated with the interactions of the Caribbean, Nazca, and South American Plates.

The analysis includes information on focal mechanisms of shallow earthquakes (depth < 60 km) reported in the global CMT catalog for the area defined by the longitudes 83.25 to 66.75° west and latitudes 4.5° south to 14.5° north. This study area encompasses the territories of Colombia, Ecuador, and Panamá and the western sector of Venezuela and covers ap-

proximately 3.9 million km² (see Figure 1 and Table 1 of the Supplementary Information).

In general, the analysis developed to obtain the orientation of the De_y and shape factor (k') includes three fundamental steps. The first step involves the preparation of information related to the earthquake focal mechanisms reported in the global CMT catalog, including changes from the "seismological" notation (azimuth, dip, and slip) to the "geological" notation (dip direction, dip, and pitch of the striae) following the right–hand rule and filtering any poorly determined solutions. Following the approaches of Frohlich & Davis (1999), any solutions in the data set for which certain tensor moment components were fixed during the inversion process ($n_{free} < 6$) are discarded, and more than 97% of the events are retained.

The second step corresponds to the application of the slip model and includes the selection of the fault plane according to the methodology of Capote et al. (1991) through the *FEX* 4.1 module developed by De Vicente & Muñoz–Martin in 1995 (personal communication). The plane that is mechanically compatible with the slip model is selected as the failure plane (De Vicente, 1988; Reches, 1978, 1983), and the values of the maximum shortening direction (De_y), friction angle (ϕ), and strain ellipsoid (k') are determined.

The last step corresponds to the construction of the De_y trajectories that represent a continuous surface with the average regional distribution of stresses (2–D distribution of vector orientation data). This study accomplishes this step by decomposing the directional point vectors into the corresponding east–west and north–south components. Subsequently, a regular mesh with representative mean values is obtained using the blockmean module of the Generic Mapping Tools (GMT) (Wessel & Smith, 1991; Wessel et al., 2013), and the interpolation to a continuous surface of variation is carried out using the GMT surface module. During this interpolation, we test different cell size values and surface tension degrees until the most representative values for the data set and map scale are identified.

Furthermore, we construct continuous maps of the stress regime using a method similar to that for the maps of De_y. Because the parameter k' is a scalar quantity that can have values between $+\infty$ and $-\infty$, the values must be normalized so that they remain in a narrower range (e.g., between 0 and 300). An average normalized k' value is obtained for each node (blockmean), and subsequent interpolations are performed on a continuous surface using the surface command.

To visually highlight the variations in the orientations of the maximum shortening direction and the stress regime and to better understand the relationships between the data and the regional morpho–structure, the results are superimposed on a shaded relief image created from a digital elevation model.

Supplementary Information includes a map showing the analyzed focal mechanisms and a table that lists the locations of the considered events (Weston et al., 2018) and information on the two nodal planes (azimuth, dip, and slip) for the focal mechanisms in the global CMT catalog analyzed in this study and used in the construction of the maximum horizontal shortening map. The results of the slip model (Reches, 1978, 1983) are listed for each individual mechanism.

2.2. Strain from the Velocity Field Obtained by Geodetic Techniques

In geodynamic studies, geodetic observations (e.g., GNSS, including GPS data) are a valuable source of data that can be used to detect, quantify, and model deformation in the Earth's crust.

Different approaches are used to derive strain information from instantaneous velocity data defined by global positioning. These approaches include those that require information on the location, slip rate, and block depth of the principal faults, whereas other approaches do not consider a priori assumptions about the fault structure and simply perform a biharmonic interpolation of each velocity component independently (Sandwell & Wessel, 2016 and references therein). One example of the second type of approach is the distance–weighted least squares procedure proposed by Shen et al. (2015), which provides an improved map of the strain rate without using previous information about locations and fault orientations.

Haines & Holt (1993) developed a method for calculating the continuous velocity gradient tensor in plate boundary zones using the bicubic spline function to interpolate scattered geodetic data, and this method has been adopted in many subsequent studies of crustal deformation (e.g., Kreemer et al., 2014). The interpolation approach of Haines & Holt (1993) and Haines et al. (2015) provides the coupling between the two horizontal velocity components, thus resulting in a more precise interpolation of the velocity and tension fields.

The horizontal gradient derived from GNSS velocities is related to the current strain rate at the surface of the Earth and is based on the principle of invariants of tensors. This gradient is independent of the frame of reference for the velocities. The geodetic data represent average values for areas of tens of square kilometers.

In regions subject to active wavelength strain greater than the spacing between GNSS stations, the strain rates and the average stress should be comparable provided that the geodetically inferred strain at the surface remains at a constant depth. In planar deformation, the principal orientations of the strain rate tensor coincide with those of the stress rate. This assumption is acceptable when limited to the brittle upper crust.

Considering that the strain tensor ε is the derivative of the velocity with respect to one orientation, standard formulas are used to calculate the components of the strain tensor:

$$\varepsilon xx = \frac{\partial vx}{\partial x}\ ,\ \varepsilon yy = \frac{\partial vy}{\partial y}\ ,\ \varepsilon xy = \frac{1}{2}\left(\frac{\partial v\chi}{\partial y} + \frac{\partial vy}{\partial x}\right)$$

For the analysis of the crustal horizontal strain, the following products of the strain gradient tensor are obtained:

- The second invariant of the strain tensor (expressed in strain by 10^{-9}/y), which is given as follows:

$$\varepsilon = \sqrt{\varepsilon_{xx}^2 + \varepsilon_{yy}^2 + 2\varepsilon_{xy}^2} \times 10^{-9}$$

- The principal components of the strain tensor, which are expressed as follows:

$$\varepsilon_{1,2} = \frac{\varepsilon_{xx} + \varepsilon_{yy}}{2} \pm \frac{1}{2}\sqrt{\left(\varepsilon_{xx} - \varepsilon_{yy}\right)^2 + 4\varepsilon_{xy}^2}$$

- The angle of the extensional strain, which can be compared with horizontal maximum shortening and is defined as follows:

$$\alpha = \frac{1}{2}\left(\frac{2\varepsilon_{xy}}{\varepsilon_{xx} - \varepsilon_{yy}}\right)$$

To calculate the uniform velocity field that coincides with the measured vectors, the methods proposed by Haines & Holt (1993) and Haines et al. (2015) are used to construct a 2–D elastic model, which is implemented as a new GMT module called gpsgridder (Sandwell & Wessel, 2016). The method is based on the green functions of an elastic body subjected to stresses in the plane. This approach ensures that elastic coupling occurs between the two horizontal velocity components in the interpolation, and this coupling can be adjusted by varying Poisson's ratio. All the singular values (measurement stations) can be used only in a subset regardless of the smallest eigenvalues in the solution, thus resulting in a smoothing of the solution.

Thus, to obtain the velocity field and the different products of the strain rate tensor, the GMT grdgradient and grdmath modules are used. The results are superimposed on a shaded relief image created from a digital elevation model to visually highlight the variations and facilitate a better understanding of the relationships with the regional morpho–structure.

Additionally, applying the proper methods for analyzing the geophysical potential fields, we obtain the total horizontal gradient (THD) of the velocity from the first derivatives in the X and Y directions. The THD expresses the speed with which the velocity changes per unit area:

$$THD = \sqrt{(\partial x * \partial x) + (\partial y * \partial y)}$$

The THD is a parameter widely used in geophysics (e.g., gravimetry and magnetism) to locate areas with laterally contrasting physical properties. Analyzing the THD of horizontal velocity can reveal the regions with maximum variation in the displacement velocity vectors (both in magnitude and in orientation). The zones of maximum gradient therefore feature greater surface strain.

3. Results

For each of the proposed methodologies, the results are obtained at a regional scale to identify the behavior of tectonic stresses. The focal mechanism analyses involve information from both continental and offshore areas and span the entire thickness of the crust, whereas the analyses of GNSS data are restricted to onshore areas.

3.1. Stress States

For the stress analysis, earthquake focal mechanisms from the global CMT catalog, which is recognized as the most complete and highest quality catalog and has systematically collected data on moderate– to large–magnitude earthquakes throughout the world since 1976, are considered. This catalog includes the following information: the locations of the hypocenter and the centroid; the seismic moment tensor expressed in its components; and the nodal planes and positions of the axes obtained from waveform modeling that considers long–period body waves (with a period greater than 40 s) from the arrival of P waves to the appearance of fundamental modes and complete surface wave trains, called mantle waves (with a period greater than 135 s), at stations recorded at teleseismic distances (between 30 and 90°) from the epicenter.

For the analysis of the crustal strain, the maximum thicknesses of the crust, and the interplate coupling areas in the subduction zones are considered, and the focal mechanisms of events with depths less than 60 km are processed, for a total of 617 mechanisms in the area of regional analysis.

As previously indicated, for each focal mechanism, a direction of maximum shortening (De_y) and a shape factor (k') value are obtained. Generally, approximately half of the focal mechanisms include some component of shear, including predominantly strike–slip faults with normal and reverse components (49%), reverse and oblique reverse faults (40%), and normal and oblique normal faults (11%).

This methodology allows the creation of a map of De_y, and the resulting map is superimposed on a representation of the type of mechanism to provide information about the ellipsoid of stresses at each point. This map presents a higher level of detail on the orientation of maximum horizontal shortening than reconstructions from stress point tensor data (Figure 3). A map of the shape factor of the strain ellipsoid is also obtained, which provides a regional view of the stress regime (e.g., extensional, shear, or compressive) in each zone (Figure 4).

These maps allow us to simply and intuitively analyze the current crustal stress state and present more continuous and higher–resolution data than those found in previous works. The extent of the analyzed area allows a comparison of the active tectonic processes associated with the plate boundaries expe-

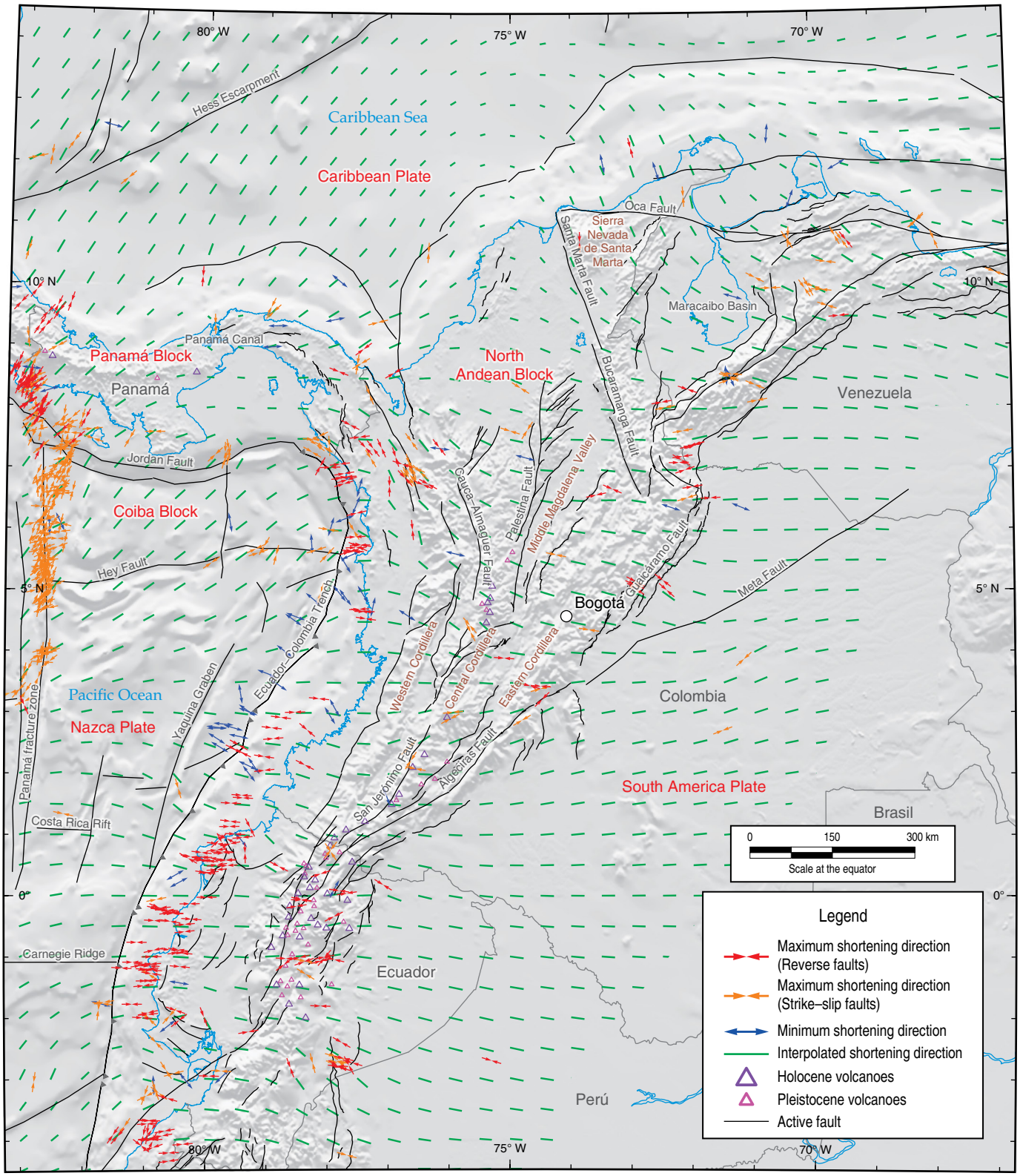

Figure 3. Map of orientations of active horizontal stresses and trajectories of the maximum horizontal shortening (De_y).

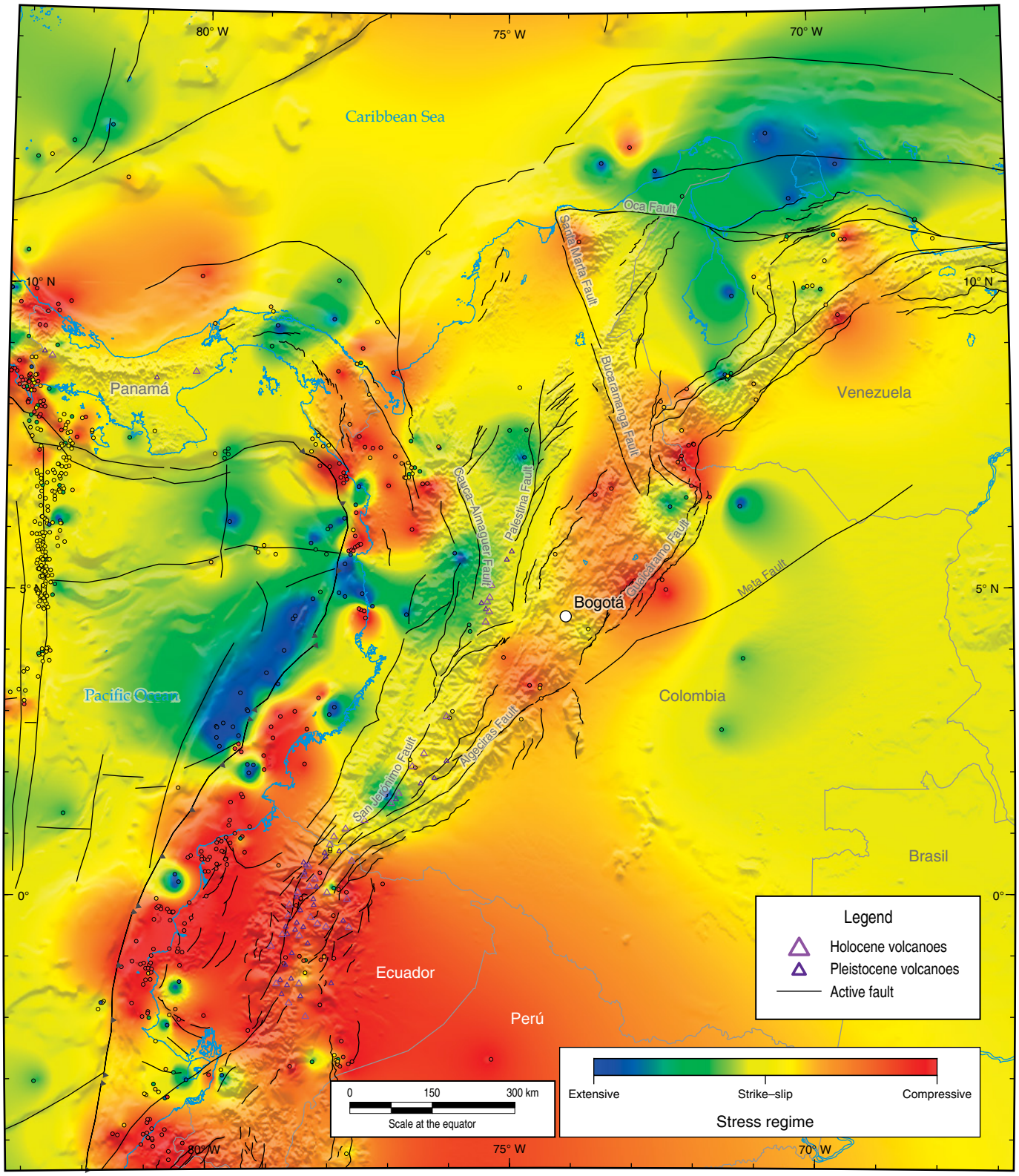

Figure 4. Map of the active stress regime represented by the shape factor (k'). The circles indicate the normalized k' value obtained for each focal mechanism.

riencing active brittle strain processes in northwestern South America and can be used to correlate the variations in the stress field with the primary generation stresses as well as the principal tectonic features and crustal heterogeneities.

3.1.1. Orientations of Maximum Horizontal Shortening

For plate boundaries, clear trends in the orientations of De_y can be identified. In the Pacific Ocean close to the Panamá fracture zone, a SW–NE trend is maintained through the Coiba Block and extends to the Caribbean Plate. In the zone next to the Ecuador–Colombia trench and to the southwest of the study area, the De_y trend effectively reflects the W–E convergence between the Nazca and South American Plates. Although this change in orientation is not particularly noticeable in the oceanic crust, it occurs near the Costa Rica Rift, which is oriented W–E and is located west of the Panamá fracture zone. The SW–NE trend south of the Carnegie Ridge is associated with subduction of the Nazca Plate to the northeast.

In the distributed strain zones within the plate interiors, large changes are recognized in the directions of De_y, and the orientations vary from NW–SE in the border area between Colombia and Panamá to W–E in the southern region of Colombia.

In the continental intraplate crust, the De_y directions radiate from two regions: the central segment of the Eastern Cordillera in Colombia and the Pacific coast in Ecuador. These trajectory configurations reflect points at which the two principal horizontal stresses are equal; that is, these areas constitute points at which the stress state is hydrostatic and are called isotropic points. Such points may represent local maxima or minima.

Another notable feature on the map presented in Figure 3 is the convergence in the orientations of De_y in the vicinity of the Colombia–Panamá border, which represents a triaxial compression zone that is the product of the convergence of the Andean, Coiba, and Panamá Blocks in this area. In this zone, the orientation of the maximum horizontal stress is the same in all directions.

In Venezuela and at the Colombian border, the orientation shifts counterclockwise from a NW–SE direction to a W–E direction in the plains area with an inflection in the mountain range, thus becoming perpendicular to the mountain chain. This change is associated with dextral transform faulting between the Caribbean and South American Plates.

To the north of Colombia, an alignment of thrust vectors associated with the maximum horizontal stress is observed, and it varies from a NW–SE orientation to the west of the serranía de San Lucas in the NW to a W–E orientation at the border with Venezuela.

3.1.2. Stress Regime

Although the distribution of the stress regimes is heterogeneous, it is related to the processes acting in the region, and the transitions between each type of stress regime are shown on the map (Figure 4). Areas with compressional regimes (red in the map) are found mainly in zones of convergence between plates and blocks, for example, at the interface between the Nazca Plate and the Andean Block off the coast of Ecuador and southern Colombia, between the Coiba and Andino Blocks in the northern Pacific region of Colombia, and between the Cocos and Caribbean Plates along the Pacific and Caribbean coasts of the Costa Rica–Panamá border.

Within the continent, the stress regime is mainly transpressional (orange on the map) in Ecuador, the center and northern segments of the Eastern Cordillera in Colombia, the eastern and western piedmonts of the Middle Magdalena Valley, and the northern and southern piedmonts of the Mérida area in the Venezuelan Andes. In the Caribbean region, a transpressional regime is also present between the Hess Escarpment and the Caribbean region of Colombia, including the western Sierra Nevada de Santa Marta mountain range.

Shear regimes (yellow) are dominant in the Panamá fracture zone, the Jordan Fault, and the Hey Fault, which define the active limits of the Coiba Block.

Transtensional regimes (green) are present in the Nazca Plate, in the area west of the Yaquina Graben, in the Coiba Block, in the central and western mountain ranges of Colombia, in the forearc zone and the northern volcanic zone of Colombia, in the area of Panamá east of the Panamá Canal and north of the Hess Escarpment, in the Maracaibo Basin, and in the eastern plains of Colombia.

An extensional regime (blue) is not common in the region and is primarily observed off the Pacific coast of Colombia, where seismicity clearly associated with the outer rise in the Nazca Plate is observed. Furthermore, extension is observed in isolated areas that possibly define zones of greater and lesser coupling at the Nazca–Andean Block interface. Similarly, local extensional fields are recognized in some of the largest sedimentary basins because of transtensional structures (pull–apart basins) and in elevated areas of mountain ranges in Colombia due to the great lithostatic load caused by the topography.

Similar results have been observed in other areas of the Andes in previous studies, such as Sébrier et al. (1985), who noted that the local stress field produces extension in topographically elevated areas (above 3000 m) and compression at lower elevations. This secondary stress field is superimposed on the state of primary compressive stress caused by the convergence of the Nazca and South America Plates, and permutations are observed between the positions of the principal axes without substantially changing their orientations. The local stresses

must be derived from instability produced by the presence of high–elevation topography and crustal roots, which produce extension perpendicular to the plateau itself.

The orientations of De_y and the described regimes are coherent with the geotectonic framework proposed by Arcila et al. (2002).

3.2. Velocities and Strain Tensor

Recognizing that geodetic measurements can also be used to estimate the strain rate tensor, a generalization of the velocity field and horizontal strain tensor for the crust in northwestern South America is obtained in this work from vectors of instantaneous velocities with respect to the fixed South American Plate determined by satellite positioning.

For the analysis, we use the most recent multiyear solution of the continental reference frame SIR15P01 from the publicly available SIRGAS network (Sánchez & Drewes, 2016a, 2016b). According to Sánchez & Drewes (2016a), SIR15P01 covers the period between 14 March 2010 and 11 April 2015 and includes the positions and velocities for 303 SIRGAS reference stations and 153 additional stations that were added to improve the geographical distribution. The solution refers to the IGb08 framework, epoch 2013.0, and has average positional precisions of ±0.7 mm/y for the north–south component, ±0.9 mm/y for the east–west component, and ±3.5 mm/y for the vertical component. In the case of the estimated velocities in the multiyear solution, the precisions are estimated to be ±0.5 mm/y for the north–south component, ±0.8 mm/y for the east–west component, and ±1.6 mm/y for the vertical component.

The SIRGAS network of continuous operation (SIRGAS–CON) is currently composed of approximately 400 stations in Latin America, and it is based on the voluntary contributions of more than 50 entities that have installed the stations and ensure proper operations. These institutions then make the observations available to the analysis centers. SIRGAS–CON forms a highly accurate geodetic infrastructure that provides the user community with essential products to satisfy needs related to positioning, navigation, cartography, and atmospheric and geodynamic studies (SIRGAS, 2007).

In this study, a map of the horizontal velocity field with respect to South America was initially generated. Because it is continuous and has a higher resolution than maps in previous works, the present map allows the rapid and easy identification of the variations in the velocities and displacement orientations that have been determined in this work (Figures 5, 6).

Generally, the northern block of the Andes in Ecuador exhibits northeastward displacement. The zone of lowest velocities (close to 5 mm/y) is in cratonic areas in Colombia, Ecuador, and Venezuela and extends to the axial zone of the Eastern Cordillera in the north, where it bifurcates to the north in Colombia and to the NE in Venezuela (Mérida Andes) and extends south to the Upper Magdalena Valley. For the westernmost sector of the Andean Block, the velocities are on the order of 10 mm/y, with higher values observed in the coastal zone of Ecuador and southern Colombia, which represents an effect of convergence with the Nazca Plate where velocities double. An area with lower velocity associated with the northern volcanic zone in Colombia is also observed. Another increase in velocities is seen in the Caribbean region of Colombia, where the orientations and velocities are associated with the displacement of the Caribbean Plate. The highest velocities (25 to 30 mm/y) are found in the Panamá Block due to the thrusting of the Cocos Plate (Figure 6).

We have also generated maps of the strain rate (second invariant of the strain tensor) and determined the principal axes of the horizontal strain tensor (Figures 7 and 8, respectively). The values of the strain rates are <100 nstrain/y in crustal zones and are highest in the Costa Rica–Panamá border area and the Andean zone of Ecuador. In Colombia, the highest values are located in the south, where the Eastern Cordillera detaches from the Western and Central Cordilleras. Other zones with significant strain rates are observed in the area bordering Ecuador, in northwestern and central Colombia, and south of Bogotá (Figure 7).

The strain tensors (Figure 8) can be identified in areas where uniaxial compressive stresses of different magnitudes dominate (e.g., the Costa Rica–Panamá border and the northwestern sector of Colombia). Hydrostatic stresses are observed in the central segment of the Eastern Cordillera in Colombia, western Panamá, and the Pacific coast in Ecuador, where the horizontal axes are equal, thus defining local maxima and minima.

The map of the total horizontal strain gradient shows the variations in the velocity changes, and the zones with higher strain rates are presented on the map of the second invariant of the strain tensor. This map highlights regions in eastern Colombia with high horizontal gradients (implying greater surface strains) that have not been well defined in previous analyses (Figure 9).

4. Discussion

This chapter presents an improved definition of the tectonic processes occurring in northwestern South America, representing an advance compared to previous studies by incorporating a higher density of information, and allows us to compare the distribution of stress at depth (focal mechanism data) and the deformation observed at the surface (GNSS data).

After providing results for each of the methodologies, an integrated analysis is performed in this section to identify the similarities and differences between them.

The projections on the map of the orientations of the strain axes (deduced from GPS velocities) and maximum horizontal

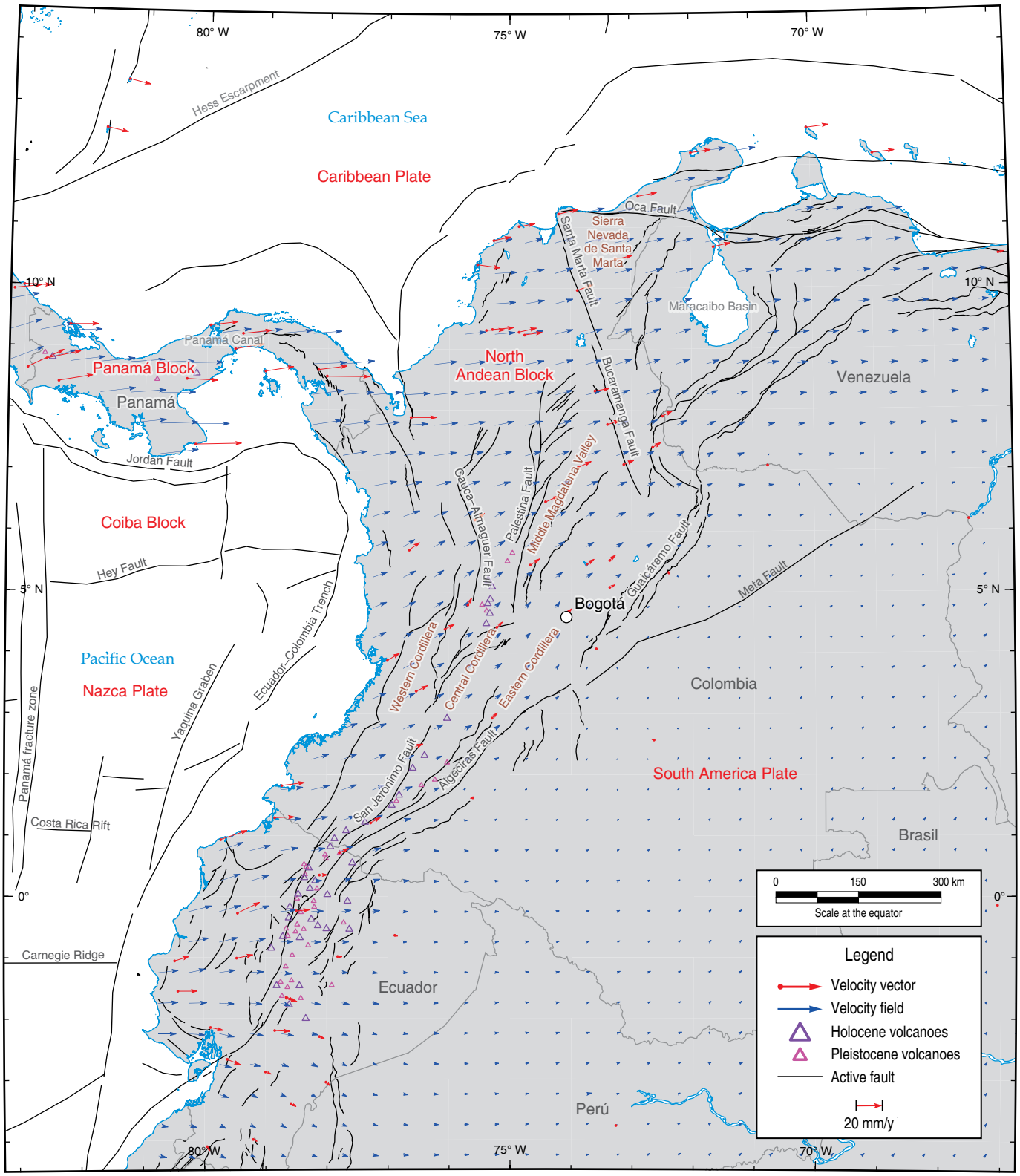

Figure 5. GNSS velocity values and resulting velocity field (with respect to the South American Plate).

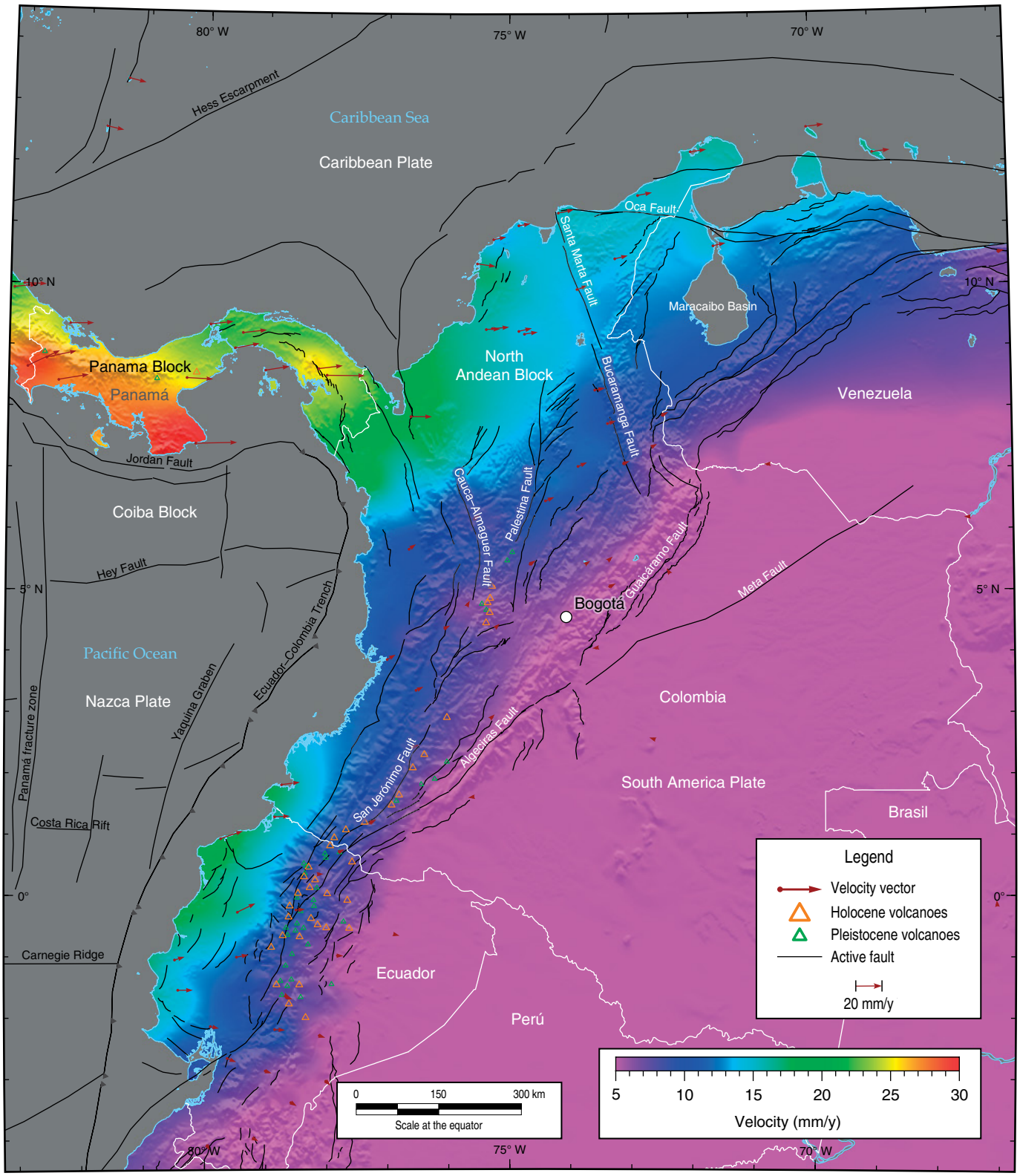

Figure 6. Interpolated map of the displacement velocity field.

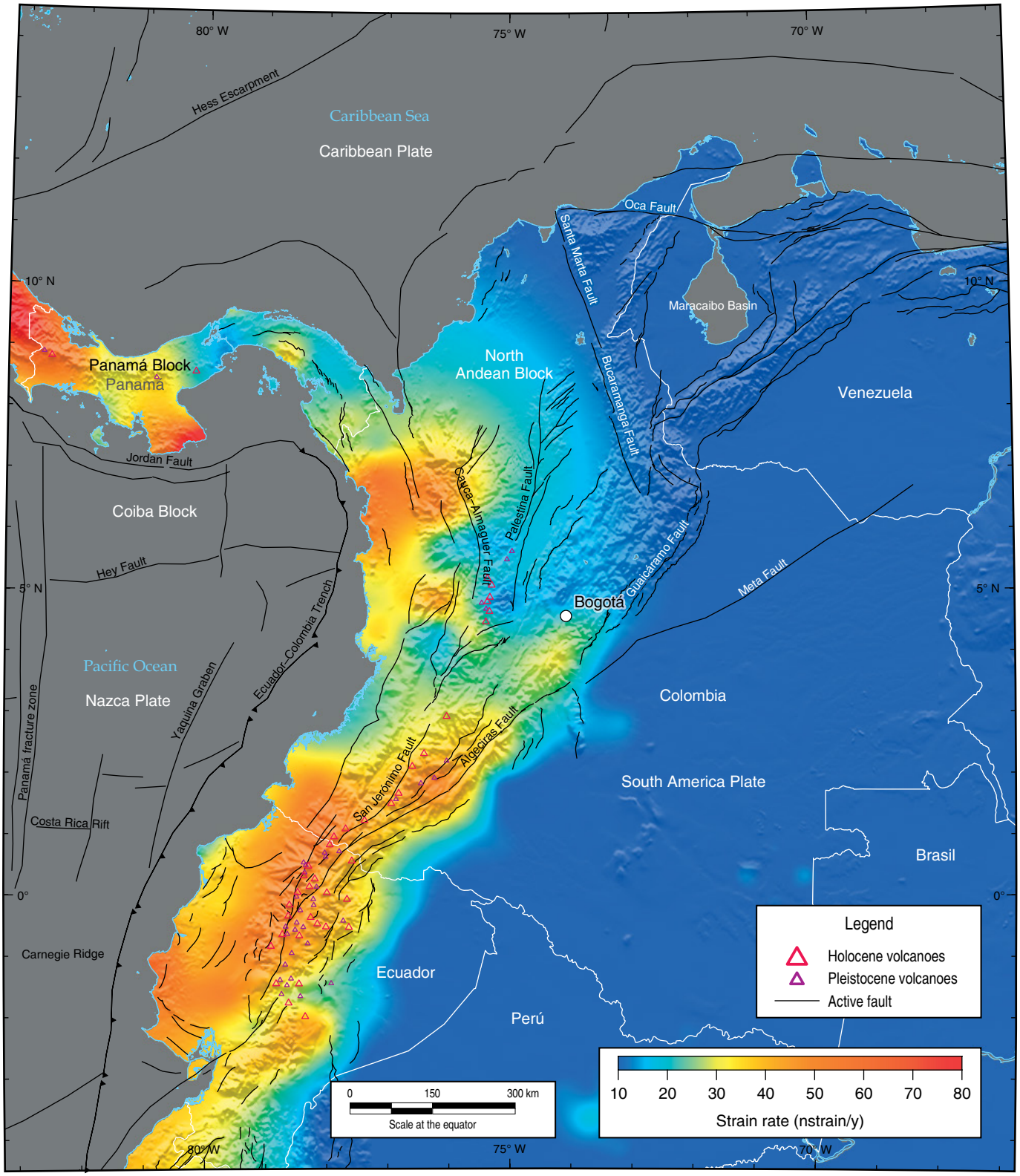

Figure 7. Strain rates (second invariant of the strain tensor).

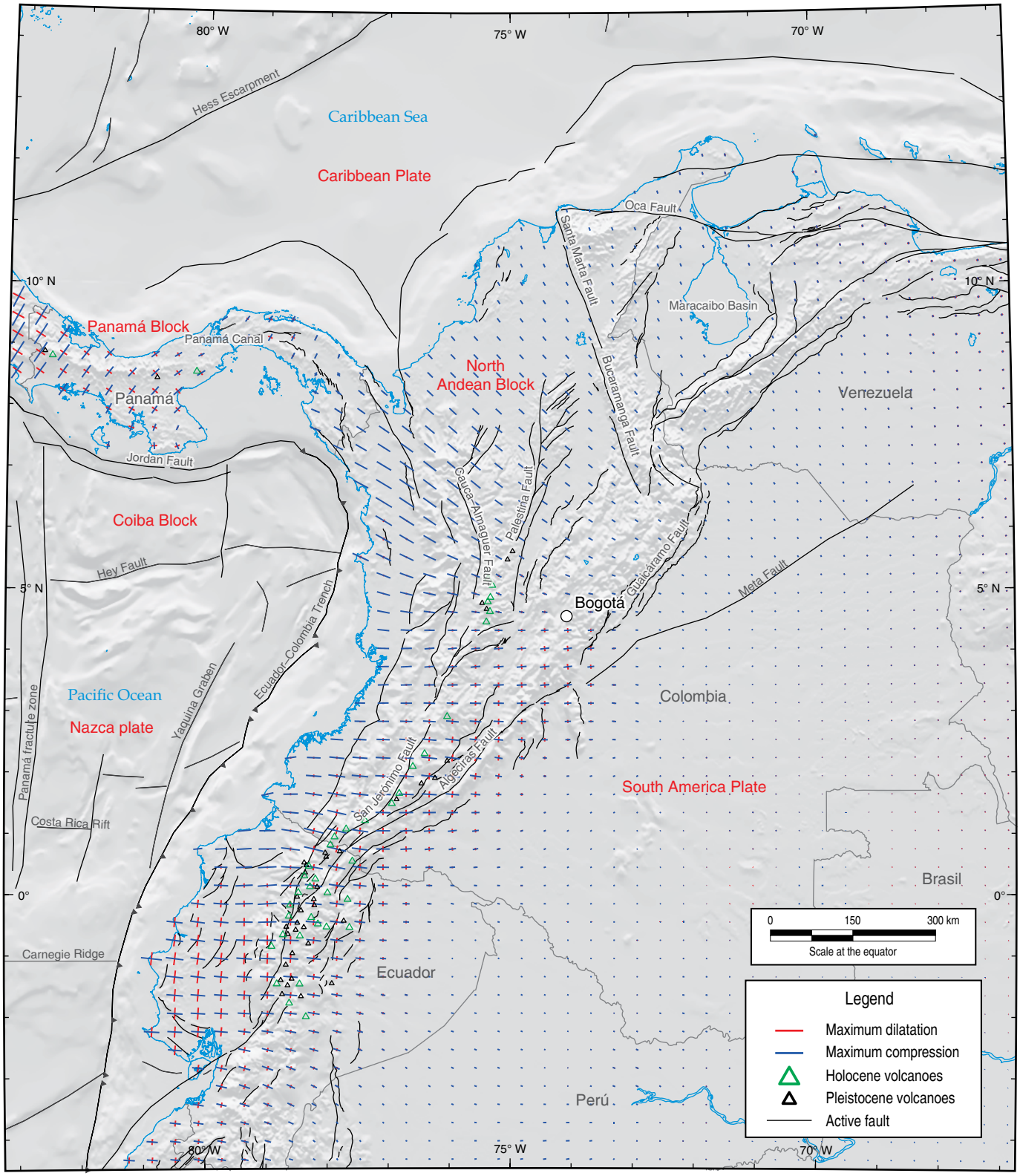

Figure 8. Orientations and magnitudes of the horizontal axes of the strain tensor defined from the GPS velocities.

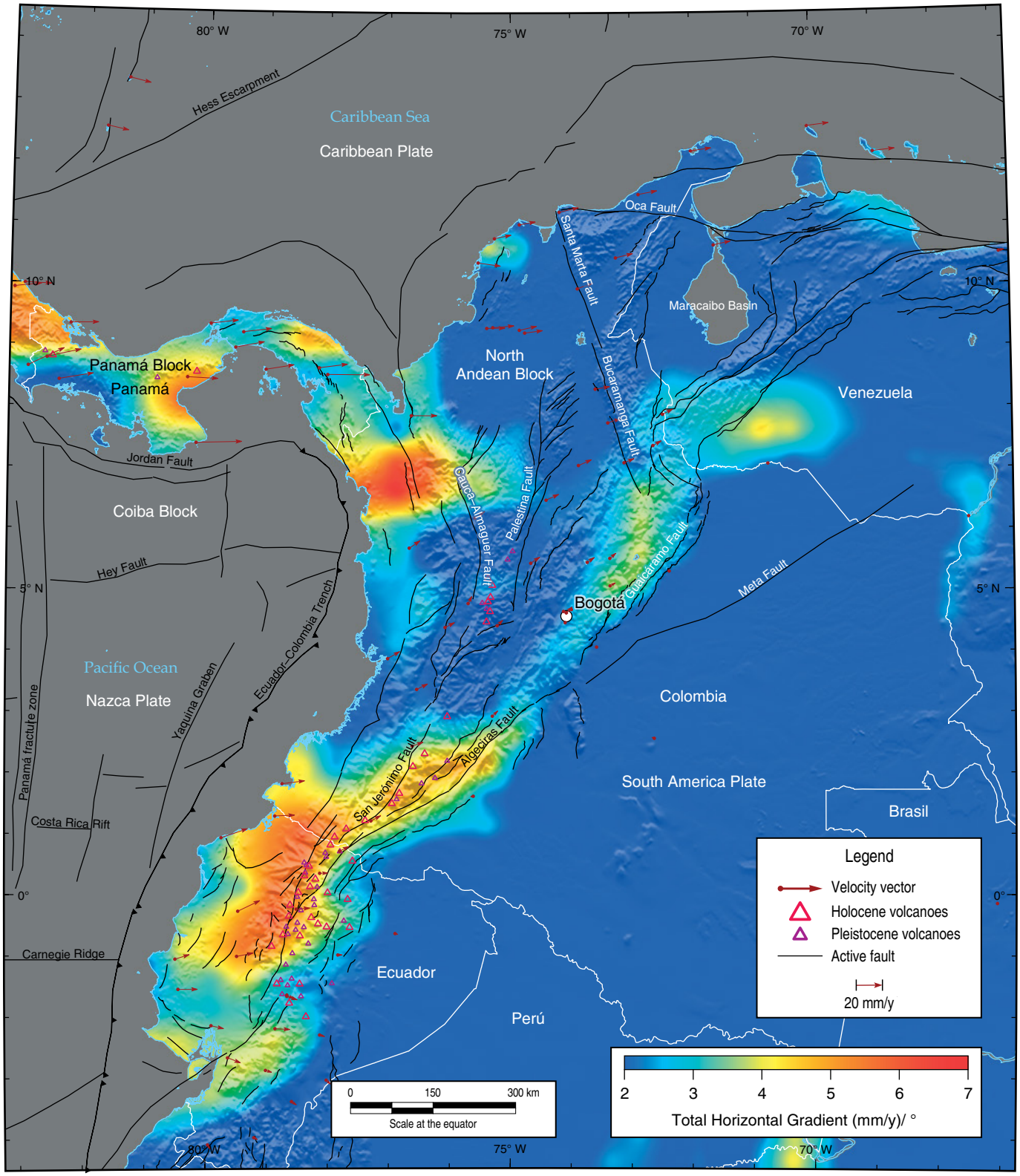

Figure 9. Total horizontal strain gradient defined from the GPS velocities.

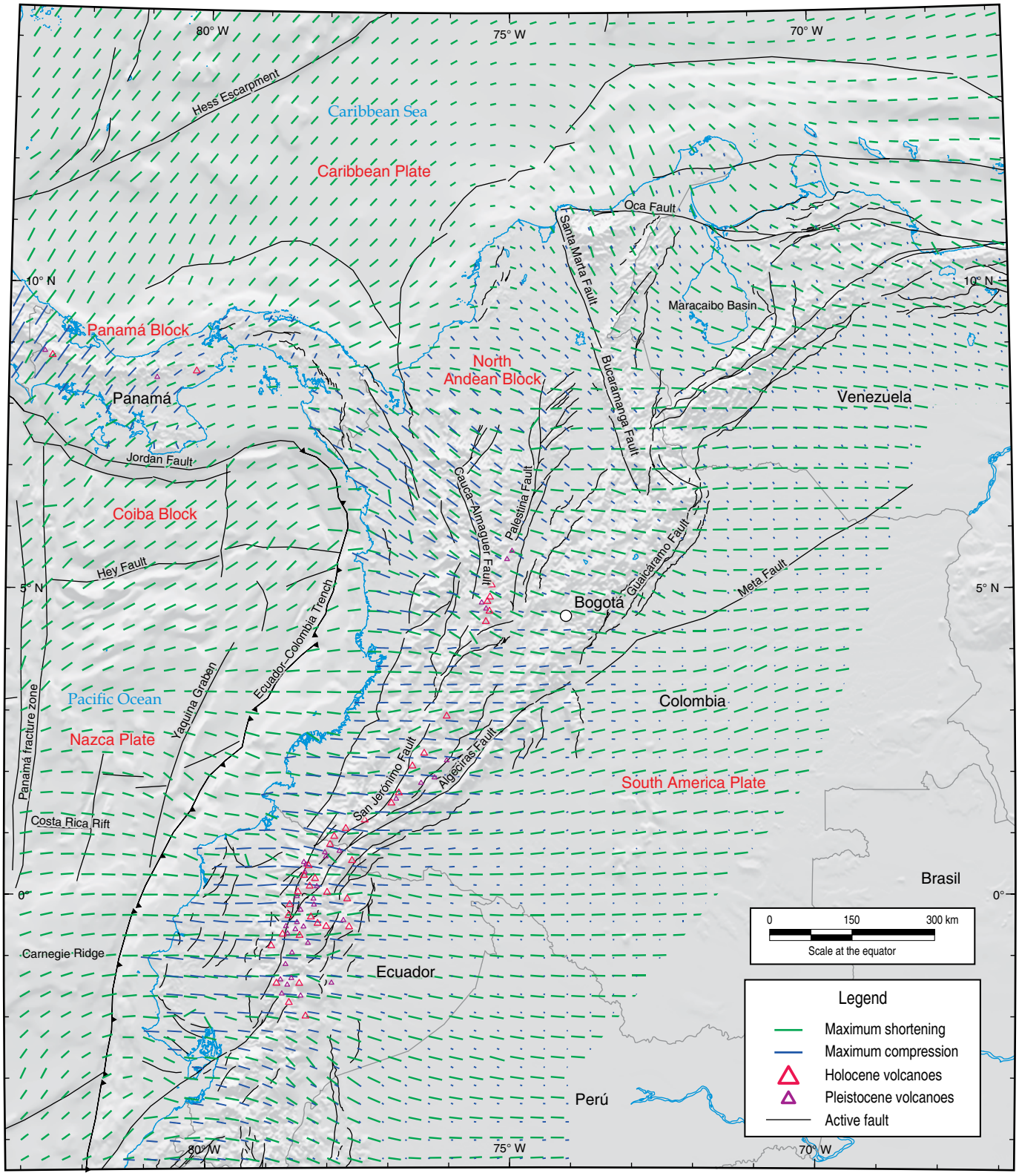

Figure 10. Orientations of the maximum horizontal shortening defined from the focal mechanism and the principal strain axis defined from the GNSS data.

shortening (De_y) (deduced from earthquakes) show very similar patterns (Figure 10). The greatest differences are found in northeastern Colombia and Venezuela, where the lowest strain rates are observed and the extensional–type regime dominates.

Although the orientations of De_y obtained from the focal mechanisms do not provide information on their magnitude, a comparison of the De_y orientations and the compressive axes deduced from the strain tensor data reveals that greater parallelism between these parameters is observed in the zones where the maximum horizontal axis is large, such as in Costa Rica and western Colombia. In areas of low strain intensity, scattered results are more likely, especially if the information is derived from sources at different depth levels.

A comparison of the stress regimes deduced from the focal mechanisms and the surface strain deduced from the GPS velocity vectors reveals that zones with higher degrees of compression are also zones with higher strain rates (second invariant). Such areas include Costa Rica Rift and the Andean region of Ecuador and Colombia, whereas an exception to this pattern is found in the northern segment of the Eastern Cordillera.

This stress regime is characterized by an increasing magnitude of deformation from east to west produced by deep processes; subduction is perpendicular in the Ecuadorian segment and oblique northwards underneath Colombia, and its effects on volcanism are evident. The volcanoes in Ecuador occur in a compressive regime, which changes to transpressive in southern Colombia, while the northern segment is extensional.

The greatest discrepancies between the two orientations and between the stress and strain regimes are observed in the northern zone between Colombia and Venezuela. Compressive stresses occur in the two mountain ranges and along the range front, and extensional stresses occur in the Maracaibo area. Maps derived from GPS data do not capture these processes. The discrepancies between the obtained results seem to be associated with the different spatial distributions of the data and the different depths from which the information was obtained, which is why the two types of data complement one another.

5. Conclusions

The joint analysis of focal mechanism data and GNSS data can be used to provide regional–scale descriptions of the dominant stress regime, the orientations of De_y, and the relationship between the stress regime and tectonics across large regions. Furthermore, this type of analysis can even show local disturbances related to crustal and topographic heterogeneities. The resulting maps also provide information on the relative magnitudes of the principal stresses.

In areas where the density of information is appropriate, the results for the directions of maximum shortening and tectonic regimes are consistent.

From the analyses, we can identify the continental zones that best accommodate the strain produced by the convergence between plates and lithospheric blocks. These areas correspond to zones that are mainly in compressional to transpressional regimes and that exhibit the highest strain rates.

In the interface zone where the dominant regime is compressional to transpressional, we can define zones that clearly exhibit coupling between the subducting Nazca Plate and the Andean Block and are separated by extensive areas with reduced coupling.

The present–day stress and strain results for the Colombian territory obtained with the slip model using earthquake focal mechanisms and strain rate tensor data show that the seismogenesis is directly related to the plate boundaries, and the results are consistent with a seismotectonic scheme characterized by the convergence of the Andean, Coiba, and Panamá Blocks in northwestern Colombia, by the W–E convergence of the Nazca and South American Plates and by the relationships between these plates and the Caribbean Plate.

Acknowledgments

We thank Laura SÁNCHEZ of the Deutsches Geodätisches Forschungsinstitut der Technischen Universität München (DGFI–TUM) for providing additional information on the solution SIR15P01. We appreciate the ability to use the GMT software developed by Wessel et al. (2013) for generating the maps and calculations. The results presented here are part of the doctoral thesis of Mónica ARCILA.

References

Anderson, E.M. 1951. The dynamics of faulting and dyke formation: With applications to Britain. Oliver and Boyd, 1913 p. Edinburgh, Scotland.

Angelier, J. 1994. Fault slip analysis and paleostress reconstruction. In: Hancock, P. (editor), Continental Deformation. Pergamon Press, p. 53–100. New York.

Arcila, M., Muñoz–Martín, A. & De Vicente, G. 2000a. Mapa de esfuerzos actuales en el bloque norte de los Andes. 2.° Asamblea Hispano Portuguesa de Geodesia y Geofísica. Extended abstract, S03–21, p. 151–152. Lagos, Portugal.

Arcila, M., Muñoz–Martín, A. & De Vicente, G. 2000b. Marco geotectónico para el noroeste de Suramérica y sur de Centroamérica. Geotemas, 1(2): 279–283.

Arcila, M., Muñoz–Martín, A. & De Vicente, G. 2002. Análisis sismotectónico de la convergencia Caribe, Nazca, Suramérica. Primer Simposio Colombiano de Sismología. Memoirs in CD ROM, 16 p. Bogotá.

Audemard, F.E. & Audemard, F.A. 2002. Structure of the Mérida Andes, Venezuela: Relations with the South America–Caribbean

geodynamic interaction. Tectonophysics, 345(1–4): 299–327. https://doi.org/10.1016/S0040-1951(01)00218-9

Bott, M.H.P. 1959. The mechanism of oblique slip faulting. Geological Magazine, 96(2): 109–117. https://doi.org/10.1017/S0016756800059987

Capote, R., De Vicente, G. & González–Casado, J.M. 1991. An application of the slip model of brittle deformation to focal mechanism analysis in three different plate tectonic situations. Tectonophysics, 191(3–4): 399–409. https://doi.org/10.1016/0040-1951(91)90070-9

Cardona, C., Salcedo, E.deJ. & Mora, H. 2005. Caracterización sismotectónica y geodinámica de la fuente sismogénica de Murindó, Colombia. Boletín de Geología, 27(44): 115–132.

Castillo, J.E. & Mojica, J. 1990. Determinación de la orientación de esfuerzos actuales a partir de deformaciones tectónicas ("breakouts") en algunos pozos petroleros de los Llanos Orientales y del Valle Medio del Magdalena, Colombia. Geología Colombiana, (17): 123–132.

Colmenares, L. & Zoback, M.D. 2003. Stress field and seismotectonics of northern South America. Geology, 31(8): 721–724. https://doi.org/10.1130/G19409.1

Corredor, F. 2003. Seismic strain rates and distributed continental deformation in the northern Andes and three–dimensional seismotectonics of northwestern South America. Tectonophysics, 372(3–4): 147–166. https://doi.org/10.1016/S0040-1951(03)00276-2

Delvaux, D. & Sperner B. 2003. New aspects of tectonic stress inversion with reference to the TENSOR program. In: Nieuwland, D.A. (editor), New insights into structural interpretation and modelling. Geological Society of London, Special Publication 212, p. 75–100. https://doi.org/10.1144/GSL.SP.2003.212.01.06

DeMets, C., Gordon, R.G. & Argus, D.F. 2010. Geologically current plate motions. Geophysical Journal International, 181(1): 1–80. https://doi.org/10.1111/j.1365-246X.2009.04491.x

De Vicente, G. 1988. Análisis poblacional de fallas: El sector de enlace Sistema Central–cordillera Ibérica. Doctoral thesis, Universidad Complutense de Madrid, 317 p. Madrid.

De Vicente, G., Cloetingh, S., Muñoz–Martín, A., Olaiz, A., Stich, D., Vegas, R., Galindo–Zaldivar, J. & Fernández–Lozano, J. 2008. Inversion of moment tensor focal mechanisms for active stresses around the microcontinent Iberia: Tectonic implications. Tectonics, 27(1): 1–22. https://doi.org/10.1029/2006TC002093

Dimaté, C., Rivera, L., Taboada, A., Delouis, B., Osorio, A., Jiménez, E., Fuenzalida, A., Cisternas, A. & Gomez, I. 2003. The 19 January 1995 Tauramena (Colombia) earthquake: Geometry and stress regime. Tectonophysics, 363(3–4): 159–180. https://doi.org/10.1016/S0040-1951(02)00670-4

Dziewonski, A.M., Chou, T.A. & Woodhouse, J.H. 1981. Determination of earthquake source parameters from waveform data for studies of global and regional seismicity. Journal of Geophysical Research: Solid Earth, 86(B4): 2825–2852. https://doi.org/10.1029/JB086iB04p02825

Egbue, O., Kellogg, J., Aguirre, H. & Torres, C. 2014. Evolution of the stress and strain fields in the Eastern Cordillera, Colombia. Journal of Structural Geology, 58: 8–21. https://doi.org/10.1016/j.jsg.2013.10.004

Ekström, G., Nettles, M. & Dziewonski, A.M. 2012. The global CMT project 2004–2010: Centroid–moment tensors for 13 017 earthquakes. Physics of the Earth and Planetary Interiors, 200–201: 1–9. https://doi.org/10.1016/j.pepi.2012.04.002

Engdahl, E.R., van der Hilst, R. & Buland, R. 1998. Global teleseismic earthquake relocation with improved travel times and procedures for depth determination. Bulletin of the Seismological Society of America, 88(3): 722–743.

Freymueller, J. T., Kellogg, J. N. & Vega V. 1993. Plate motions in the North Andean region. Journal of Geophysical Research: Solid Earth, 98 (B12), 21853–21863 https://doi.org/10.1029/93JB00520

Frohlich, C. & Davis, S. D. 1999. How well constrained are well–constrained T, B, and P axes in moment tensor catalogs? Journal of Geophysical Research: Solid Earth, 104(B3): 4901–4910. https://doi.org/10.1029/1998JB900071

Global Volcanism Program. 2013. Volcanoes of the world. In: Venzke, E. (editor), Smithsonian Institution, version 4.7.1 (consulted in July 2018). https://doi.org/10.5479/si.GVP.VOTW4-2013

Haines, A.J. & Holt, W.E. 1993. A procedure for obtaining the complete horizontal motions within zones of distributed deformation from the inversion of strain rate data. Journal of Geophysical Research: Solid Earth, 98(B7): 12057–12082. https://doi.org/10.1029/93JB00892

Haines, A.J., Dimitrova, L.L., Wallace, L.M. & Williams, C.A. 2015. Enhanced surface imaging of crustal deformation: Obtaining tectonic force fields using GPS data. Springer Briefs in Earth Sciences, 99 p. https://doi.org/10.1007/978-3-319-21578-5

Heidbach, O., Rajabi, M., Reiter, K. & Ziegler, M, WSM Team. 2016. World Stress Map Database Release 2016. GFZ Data Services. http://doi.org/10.5880/WSM.2016.001

International Seismological Centre. 2019. ISC–EHB dataset. https://doi.org/10.31905/PY08W6S3

Kellogg, J.N. & Vega, V. 1995. Tectonic development of Panamá, Costa Rica, and the Colombian Andes: Constraints from Global Positioning System geodetic studies and gravity. In: Mann, P. (editor), Geologic and tectonic development of the Caribbean Plate boundary in southern Central America. Geological Society of America, Special Paper 295, p. 75–90. Boulder, USA. https://doi.org/10.1130/SPE295-p75

Kreemer, C., Blewitt, G. & Klein, E.C. 2014. A geodetic plate motion and global strain rate model. Geochemistry, Geophysics, Geosystems, 15(10): 3849–3889. https://doi.org/10.1002/2014GC005407

McKenzie, D.P. 1969. The relation between fault plane solutions for earthquakes and the directions of the principal stresses. Bulletin of the Seismological Society of America, 59(2): 591–601.

Muñoz–Martín, A., Cloetingh, S., De Vicente, G. & Andeweg, B. 1998. Finite–element modelling of tertiary paleostress fields in the eastern part of the Tajo Basin (central Spain). Tectonophysics, 300(1–4): 47–62. https://doi.org/10.1016/S0040-1951(98)00233-9

Olaiz, A.J., Muñoz–Martín, A., De Vicente, G., Vegas, R. & Cloetingh, S. 2009. European continuous active tectonic strain–stress map. Tectonophysics, 474(1–2): 33–40. https://doi.org/10.1016/j.tecto.2008.06.023

Reches, Z. 1978. Analysis of faulting in three–dimensional strain fields. Tectonophysics, 47(1–2): 109–129. https://doi.org/10.1016/0040-1951(78)90154-3

Reches, Z. 1983. Faulting of rocks in three–dimensional strain fields II. Theoretical analysis. Tectonophysics, 95(1–2): 133–156. https://doi.org/10.1016/0040-1951(83)90264-0

Reches, Z., Baer, G. & Hatzor, Y. 1992. Constraints on the strength of the upper crust from stress inversion of fault slip data. Journal of Geophysical Research: Solid Earth, 97(B9): 12481–12493. https://doi.org/10.1029/90JB02258

Rivera, L.A. 1989. Inversion du tenseur des contraintes et des mécanismes au foyer à partir des données de polarité pour une population de séismes: Application a l'etude du foyer de sismicite intermediaire de Bucaramanga (Colombie). Doctoral thesis, Université Louis–Pasteur de Strasbourg, 266 p. Strasbourg, France.

Salcedo–Hurtado, E. 1995. Deformación sísmica en las zonas sismoactivas de Chocó y el "nido" de Bucaramanga. Boletín Geológico, 35(1): 51–66.

Sánchez, L. & Drewes, H. 2016a. Crustal deformation and surface kinematics after the 2010 earthquakes in Latin America. Journal of Geodynamics, 102: 1–23. https://doi.org/10.1016/j.jog.2016.06.005

Sánchez, L. & Drewes, H. 2016b. Crustal deformation and surface kinematics after the 2010 earthquakes in Latin America. PANGAEA, Data publisher for Earth & environmental science. https://doi.org/10.1594/PANGAEA.863132

Sandwell, D.T. & Wessel, P. 2016. Interpolation of 2–D vector data using constraints from elasticity. Geophysical Research Letters, 43(20): 10703–10709. https://doi.org/10.1002/2016GL070340

Sébrier, M., Mercier, J.L., Mégard, F., Laubacher, G. & Carey–Gailhardis, E. 1985. Quaternary normal and reverse faulting and the state of stress in the Central Andes of south Peru. Tectonics, 4(7): 739–780. https://doi.org/10.1029/TC004i007p00739

SIRGAS. 2007. Red de referencia. http://www.sirgas.org/es/sirgas-con-network/ (consulted in November 2019)

Shen, Z.K., Wang, M., Zeng, Y. & Wang, F. 2015. Optimal interpolation of spatially discretized geodetic data. Bulletin of the Seismological Society of America, 105(4): 2117–2127. https://doi.org/10.1785/0120140247

Stephan, J.F. 1982. Évolution géodynamique du domaine Caraïbe, Andes et chaîne Caraïbe, sur la tranversale de Barquisimeto (Venezuela). Doctoral thesis, University Pierre y Marie Curie, 512 p. Paris.

Stephan, J.F., Blanchet, R. & De Lepinay, B. M. 1986. Northern and southern Caribbean festoons (Panamá, Colombia–Venezuela and Hispa–Niola–Puerto Rico), interpreted as pseudosubductions induced by the east–west shortening of the pericaribbean continental frame. In: Wezel, F.C. (editor) The Origin of Arcs. Developments in Geotectonics, 21: p. 401–422. https://doi.org/10.1016/b978-0-444-42688-8.50022-9

Trenkamp, R., Kellogg, J.N., Freymueller, J.T. & Mora, H. 2002. Wide plate margin deformation, southern Central America and northwestern South America, CASA GPS observations. Journal of South American Earth Sciences, 15(2): 157–171. https://doi.org/10.1016/S0895-9811(02)00018-4

Vargas, C.A., Pujades, L.G., Ugalde, A. & Canas, J.A. 2002. Estado de deformación y esfuerzos en el territorio colombiano. Revista de la Academia Colombiana de Ciencias Exactas, Físicas y Naturales, 26(100): 373–391.

Veloza, G., Styron R., Taylor, M. & Mora, A. (2012). Open–source archive of active faults for northwest South America. Geological Society of America Today, 22 (10): 4–10, https://doi.org/10.1130/GSAT-G156A.1

Wessel, P. & Smith W.H.F. 1991. Free software helps map and display data. EOS, Transactions American Geophysical Union, 72(41): 441–445. https://doi.org/10.1029/90EO00319

Wessel, P., Smith, W.H.F., Scharroo, R., Luis, J. & Wobbe, F. 2013. Generic mapping tools: Improved version released. EOS, Transactions American Geophysical Union, 94(45): 409–410. https://doi.org/10.1002/2013EO450001

Weston, J., Engdahl, ER., Harris, J., Di Giacomo, D. & Storchak, D.A. 2018. ISC–EHB: Reconstruction of a robust earthquake data set. Geophysical Journal International, 214(1): 474–484. https://doi.org/10.1093/gji/ggy155

Zoback, M.L. 1992. First– and second–order patterns of stress in the lithosphere: The World Stress Map Project. Journal of Geophysical Research: Solid Earth, 97(B8): 11703–11728. https://doi.org/10.1029/92JB00132

Zoback, M.L., Zoback, M.D., Adams, J., Assumpçao, M., Bell, S., Bergman, E.A., Blümling, P., Brereton, N.R., Denham, D., Ding, J., Fuchs, K., Gay, N., Gregersen, S., Gupta, H.K., Gvishiani, A., Jacob, K., Klein, R., Knoll, P., Magee, M., Mercier, J.L., Müller, B.C., Paquin, C., Rajendran, K., Stephansson, O., Suarez, G., Suter, M., Udias, A., Xu, Z.H. & Zhizhin, M. 1989. Global patterns of tectonic stress. Nature, 341(6240): 291–298. https://doi.org/10.1038/341291a0

Explanation of Acronyms, Abbreviations, and Symbols:

CMT	Centroid–moment tensor
De_y	Maximum horizontal shortening
e_y	Axis of maximum horizontal shortening
e_z	Axis of vertical strain
DGFI–TUM	Deutsches Geodätisches Forschungsinstitut der Technischen Universität München
GMT	Generic Mapping Tools
GNSS	Global Navigation Satellite System
GPS	Global Positioning System
IGb08	IGS terrestrial reference frame
k'	Ellipsoid shape factor
Mw	Moment magnitude
P	Compression axis
R	Rake
SIR15P01	Solución multianual
SIRGAS	Sistema de Referencia Geocéntrico para las Américas
SIRGAS–CON	SIRGAS network of continuous operation
T	Tension axis
THD	Total horizontal gradient
UCM	Universidad Complutense de Madrid
ε	Strain tensor
ϕ	Internal friction angle

Authors' Biographical Notes

Mónica ARCILA is a geologist from the Universidad de Caldas and PhD student in geology and geological engineering at the Universidad Complutense de Madrid, España. She has worked with the Servicio Geológico Colombiano (SGC) since 1991 and was initially involved in volcanic surveillance activities. As a project manager in 1993, she consolidated the Observatorio Volcanológico y Sismológico de Popayán of the SGC. Since 2003, she has been studying seismotectonics for earthquake risk assessment and is currently leading these evaluations in the framework of the research applied to geological threats and risks for the Dirección de Geoamenazas.

Alfonso MUÑOZ–MARTÍN has PhD in geological sciences from the Universidad Complutense de Madrid (UCM). Since 1997, he has been a professor in the Departamento de Geodinámica at UCM. He is the director of the "Applied Tectonophysics" consolidated research group at UCM, whose lines of research are geophysics, tectonics, and marine geology. He has participated in more than 20 national and international competitive projects, serving as principal investigator for three of them. He has conducted applied research in the areas of geological engineering, mining, hydrocarbon exploration, CO_2 storage, environmental studies, hydrogeology, and archeology. Moreover, he is the author of more than 40 articles published in international journals, 16 chapters in national and international books, more than 60 publications in national journals, more than 60 papers presented at national and international congresses, and several official cartographies. He is a reviewer for national and international journals and associate editor of the Journal of Iberian Geology.

Bogotá, Colombia
2020